Infrared Supercontinuum Generation in Cladding of a Hollow-Core Fiber Pumped with a 1-ns 1.06-μm Nd^{3+}:YAG/Cr^{4+}:YAG Microchip Laser

Alexander V. Kiryanov[*,1,2], Vladimir P. Minkovich[2], Igor V. Mel'nikov[1] and Alexander B. Sotsky[3]

[1]*Optolink Ltd., Bldg. 5, Proezd 4806, Zelenograd, Moscow 124498, Russian Federation*

[2]*Centro de Investigaciones en Óptica, Loma del Bosque 115, Col. Lomas del Campestre, León 37150, Guanajuato, Mexico*

[3]*Kuleshow State University, pr. Kosmonavtov 1, Mogilev 212022, Belarus*

Abstract: We present an experimental treatment for the super-continuum (SC) generated through a hollow-core fiber by a nanosecond pulse launched from a Q-switched microchip Nd^{3+}:YAG/Cr^{4+}:YAG laser. The SC spectrally spans over a half-octave in near IR (~1.0–1.5 μm) and is attainable yet at fairly moderate fiber length (tens of cm). The SC generation process is shown to originate from silica nodes of the fiber cladding ("secondary cores"), where the pump radiation is tightly focused, and to be triggered out by a four-wave mixing process, which is boosted up by the Raman response in the fiber.

Keywords: Supercontinuum generation, hollow-core photonics crystal fiber, microchip laser.

1. INTRODUCTION

In the past decade, highly nonlinear photonic crystal fibers (PCF) have been recognized as a powerful and versatile tool for laser spectral broadening [1-3]. These fibers propagate light along a small solid core surrounded by an array of larger air holes. The nonlinear optical properties of these structures are very much akin those of a rod of glass surrounded by air, stemming from strong confinement of the light within the structure and correspondingly a large nonlinearity to arise. The modulation instability, four-wave mixing, Raman scattering, and coupling with dispersive waves are the main effects [4-7] responsible for the ultra-wide spectral broadening or supercontinuum generation (SCG) in highly nonlinear PCF when a narrow pump laser line spans up to an octave.

On the other hand, hollow-core fibers (HCF) have a lower fiber nonlinearity that, in turn, enables distortionless light delivery from powerful lasers onto a target [8-10]. Since the light guidance here occurs in a hollow core with a low attenuation, reduced nonlinearity, and much higher damage threshold, these fibers can be a valuable tool for communications, laser-spark engines, and other applications.

The SCG in standard fibers was observed more than 30 years ago [11] and so had been extensively studied through the 80-90s. The interest in this nonlinear phenomenon has been dramatically fueled by the invention of PCF (see, e.g., Refs. [12-16]), where SCG was reached at properly engineered structure of air holes in silica. Although the SCG in a PCF is typically observed with picosecond (ps) and femtosecond (fs) pump sources [17-19], some recent studies have also revealed it even at a CW pump [20]. The current state of the art and possible applications of SCG in PCF and PCF-based lasers are summarized in Refs. [1, 21-24]. Except of a single publication [25], all the aforementioned studies have been dealing with the PCF where a small silica core is surrounded by air-silica cladding of hexagonal (holey) structure that defines wave-guiding properties of the fiber. Such small size of the PCF core provides a high efficiency of the nonlinear processes involved into the SCG.

Meanwhile, the HCF with a hollow air-filled core and cladding of generally the same structure as in the highly nonlinear PCF has emerged and is being explored. In the sense of the SCG prospects, the HCF has not been considered as a suitable choice because of a quite large core size and negligible nonlinear effects that take place in the air-filled hollow core. However, Ref. [25] has reported for the first time the white-light (or SC) generation in a HCF, which is suggested to happen in "secondary cores" of the fiber cladding. In this work, a ps VIS (green) laser source was used, and the SC started to be generated at both the red and blue wings of the laser line. The authors attributed the SCG due to an efficient four-wave mixing process with phase matching reached owing to the fiber-cladding birefringence.

In the present paper, we investigate the properties of SCG in a HCF, where the SC is generated through the cascade of nonlinear processes (Raman scattering, self-phase modulation, and four-wave mixing) initiated inside the fiber cladding by a nanosecond (ns) 1.06-μm Q-switched microchip Nd^{3+}:YAG/Cr^{4+}:YAG laser. Analyzing how the whole set of SC characteristics such as spectrum span, threshold, and spatial profile depend on the fiber length and pump power, we arrive to the conclusion that a proper choice of the pump light – fiber sample coupling arrangement is the key point for highly efficient SCG in the fiber.

Notice that our results somewhat resemble those of Ref. [25]; however we would stress out the differences: (a) the

*Address correspondence to this author at the Centro de Investigaciones en Óptica, Loma del Bosque 115, Col. Lomas del Campestre, León 37150, Guanajuato, Mexico; Tel: +52 477 441-4200; Fax: +52 477 441-4209; E-mail: kiryanov@cio.mx

1874-3285/10

HCF we manufactured is of the lower air-filling factor, which meanwhile demonstrates certain potential for the SCG; (b) the SCG is initiated in our case at a different wavelength (1.06 μm) yet most common in a lab, and at quite a different time scale (ns); (c) we provide the reader with a comprehensive information on the threshold, spectral, and spatial features of near-IR SCG in the fiber.

It is also noticeable that the design proposed here provides a basis for producing both multi-color and extreme-to-low power nonlinear devices. Indeed, the band-gap property (see below) at one wavelength provided for the central air-filled hole suggests high-power light delivery by the fiber to the target which state and/or location can be simultaneously monitored by the secondary core-generated eye-safe SC. In addition, we used standard fiber drawing technique for producing a structure generating a high-quality SC at significantly lower cost than tapering and dispersion shifting-based microstructures. These open up a wider door for such application as biomedical imaging, laser surgery, and laser-induced process diagnostics.

2. EXPERIMENTAL ARRANGEMENT

The HCF is manufactured in the Centro de Investigaciones en Optica (CIO, Mexico) by the standard drawing method (see, e.g. [26]) from a preform composed of a stack of capillary tubes surrounding one removed capillary in the center of the stack. The cladding of the fiber consists of four hexagonal rings of air holes with an average diameter of 5.0 μm and a spacing of 8.0 μm, respectively. The diameter of the central hollow core is 7.5 μm at 125-μm outer diameter of the fiber. The size of silica triangular nodes composing the cladding holey web is approximately 3.0 μm. The correspondent air-filling factor for the cladding area is about 0.6-0.7. It is noticeable that the engineered group velocity dispersion (GVD) supports a "super mode" regime for the HCF holey cladding (see Fig. **1**) and, in the same time, the band-gap properties of the central (hollow) area; this makes our HCF a good choice for an effective SCG in "secondary cores" of cladding (near 1.06 μm, a zero dispersion wavelength, see Fig. **1**) and also for distortionless delivery of high-power visible light through the hollow core (see below).

The HCF image obtained at white-light illumination and registered with a microscope with a digitized output (*DC3-163 National microscope / National Magnaview video camera)* is shown in Fig. (**2**) (we used in this case short-length fiber pieces, of about 1 cm).

It is clearly seen here that the fiber hollow core transmits visible radiation, which we can assign to the presence of a band gap in the green (on the photograph, we show the case where white light was intentionally focused into the fiber core, but it was collected from a whole fiber end). It is also seen that the elements of the fiber cladding, that is, small silica triangles in the holey cladding, are highly transparent for white light too, with almost no spectral filtering to happen. In what follows, the cladding in our fiber works as a standard PCF where the role of cores is played by cladding triangular silica nodes.

Let us notice that a separate experiment was done on propagation SC light from a commercial ps source in the HCF and similar results were obtained: The secondary cores effectively propagate the SC along the fiber length. This observation suggests our HCF itself to be a source of SC at a properly pump arrangement (see Section 3).

3. RESULTS AND DISCUSSION

The results of measurements of attenuation spectra of our HCF are shown in Fig. (**3**), where Fig. (**3a**) shows the attenuation over a wide spectral range (500–1550 nm), whilst Fig. (**3b**) zooms the fiber transmission in the visible (green). The measurements were performed by focusing a weak-power white-light source (*Fianium SC400*) onto the HCF cleaved cut by using a lens and recording the transmitted

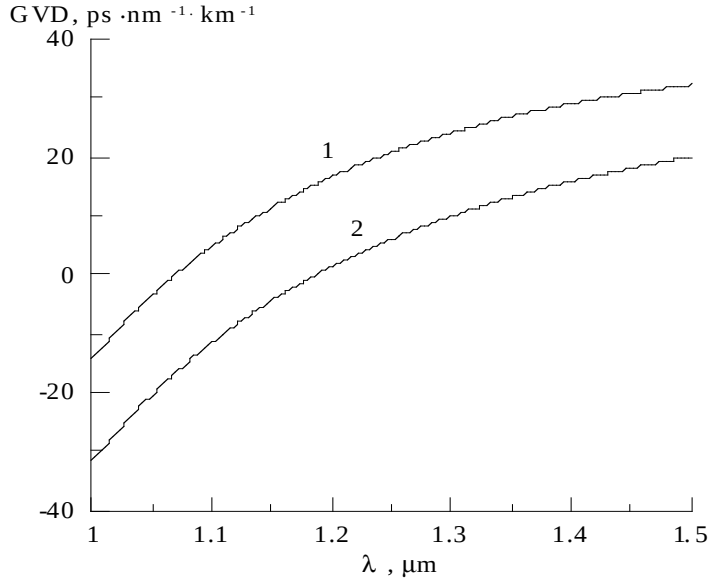

Fig. (1). Calculated GVDs for a super-mode propagating in silica triangles of cladding of HCF under scope (curve 1) and (for comparison) for the lowest mode of standard PCF with a single solid core (curve 2). The calculations have been made using the 3-terms Sellmeier equation.

light with an optical spectrum analyzer (OSA) *Yokogawa AQ6370*; notice that the spectra are obtained by subtracting the incident white-light spectrum from the measured ones.

In the attenuation spectra measurements, relatively long pieces of tens of cm of the HCF were inspected, and a transmission window is seen in Fig. (**3b**) near 547 nm. This is due to the fiber hollow core but the transmission of the fiber as a whole is essentially due to the cladding secondary cores [see Fig. (**3a**)]. The dips in the loss seen at 1250 and 1350–1450 nm, as well as less pronounced ones at 950 and 1150 nm, are most probably due to the absorption by OH overtones in the air that fills the fiber cladding holes [27].

One can also see from Figs. (**1, 2** and **3**) that properly organized focusing of the incident pump with wavelength nearby 1000 nm, that is the case of Nd or Yb lasers, can be very much favorable for the SC to be generated within the small-area silica secondary cores. In what follows, we have performed an experiment where the pump is launched into the cladding area of the HCF at the special focusing arrangement shown in Fig. (**4**).

Our main experiments on SC generation were performed with an in-house made Nd^{3+}:YAG/Cr^{4+}:YAG microchip laser operating in a hybrid active-passive Q-switching regime [28]. The microchip laser was pumped with a standard 806-nm semiconductor diode. The microchip laser delivers 1.2-ns

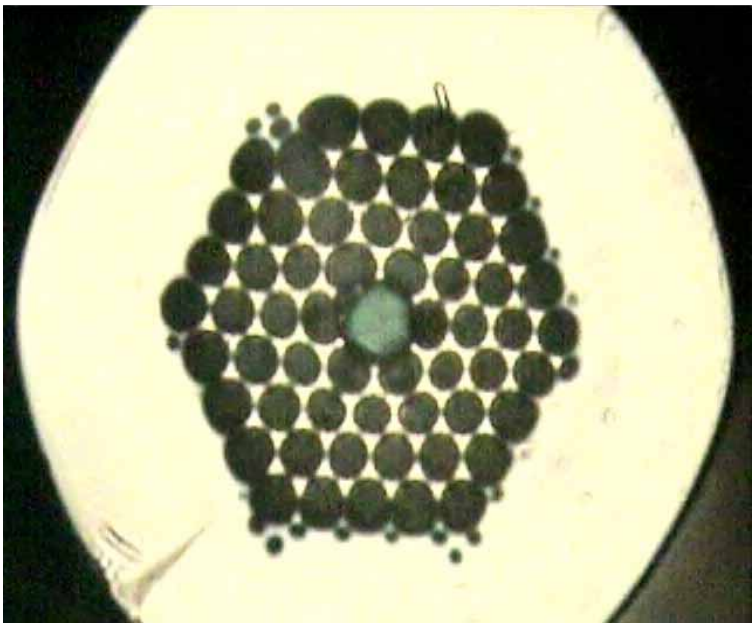

Fig. (2). HCF cleaved end image at white-light illumination (fiber length L = 1 cm).

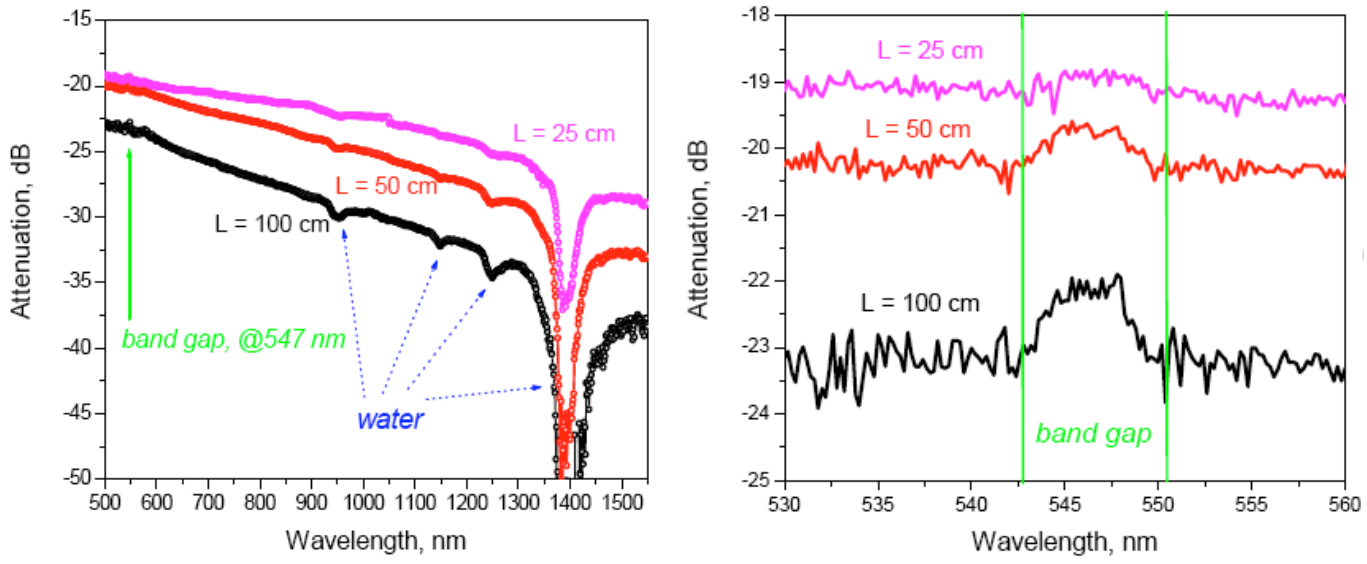

Fig. (3). HCF transmission spectra obtained for different sample length. (**a**) Overall view; (**b**) insight to a transmission window centered at @547 nm.

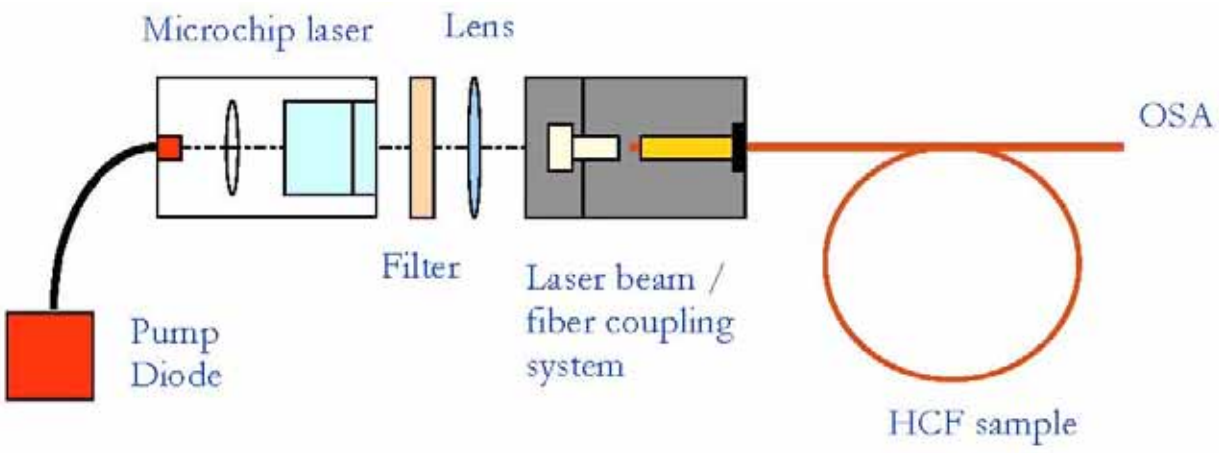

Fig. (4). Experimental arrangement.

pulses, which carry energy of 21 μJ at a controllable (1–10 kHz) repetition rate. The laser output is single-mode and single-polarization, so that no special control has to be taken over the state of polarization. The linewidth of the laser was measured to be less than ~0.2 nm.

The pump radiation was coupled to the HCF sample using the simplest optical components (see Fig. **4**) to engineer the size and power of the input beam. The pump pulse was tightly focused onto the HCF facet through an AR-coated (@1064 nm) focusing lens (f = 5 cm) followed by an objective (X 20, NA = 0.65). This enabled us to focus the pump down to the 2.5–3-μm focal diameter and so to couple the pump into one of the silica triangular nodes which compose the fiber cladding.

The signal on the HCF output was analyzed with an OSA (*Yokogawa AQ6370* or *Ando AQ 6315A*), photo-detector (*Red Wave D123*), and power-meter (*Anritsu ML 910B*). In the experiments, we exploited different pieces of the fiber samples with length varied from 15 to 250 cm; the incident pump power was varied as well.

Our main results on the SCG in the HCF are highlighted at Figs. (**5-8**) below.

Let us start with the length and pump energy dependences; the later is obtained by placing the neutral filters in front of the focusing lens.

Fig. (**5**) presents the two most typical scenarios of the SCG at different fiber lengths and pump energy delivered by the microchip laser to the fiber. It is seen that the SC is effectively generated within a 950–1450 nm half-octave provided the fiber is long enough (tens of cm). The other observation from Fig. (**5**) illuminates the physical processes that take place in the silica triangle cladding, behind this generation. The offset of the modulational instability is readily observed at the shorter fiber length. These sidebands are enhanced by the pump and spread the pulse spectrum to the Stokes side, which is defined by the action of Raman self-scattering. The longer the fiber is the larger numbers of sidebands are generated between the Stokes components that results in the smooth step-like half-octave spectral profile with no fringes imposed. That is, the SC spans through the

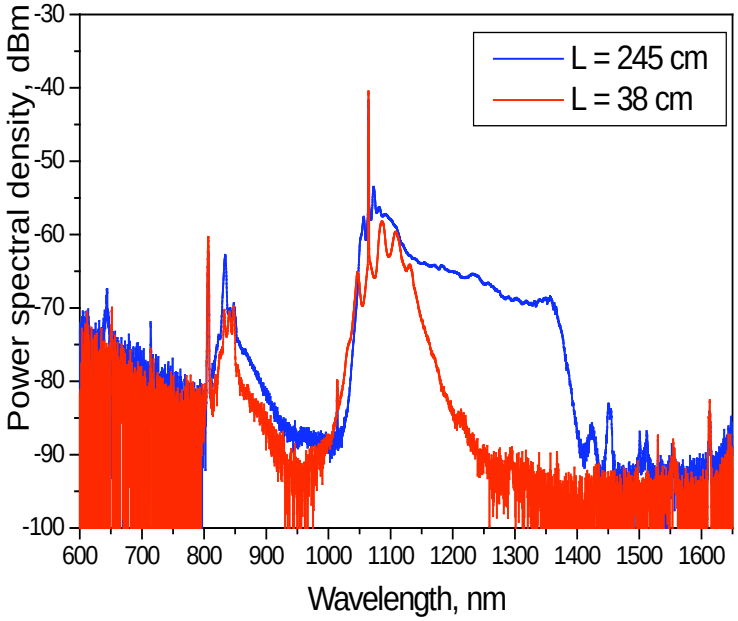

Fig. (5). SC spectra recorded at two different HCF lengths (L = 38 and 245 cm) and maximal (10 μJ) pump power delivered to the fiber.

whole gap of the HCF high (cladding) transparency region and has a red bound that is due to the water absorption around 1450 nm. It is also worth noticing the remnants of the diode pump centered at 806 nm, seed up the less intense 100-nm SC spanning from 800 to 950 nm.

In turn, Fig. (**6**) suggests additional proofs in favor of both the self-phase modulation as a SC start-up mechanism [see Fig. (**6a**)] and Raman self-scattering whose strong 1st, 2nd, and 3rd maximums shift the narrow pump line over this half-octave [see Fig (**6b** and **c**)]. Here the SC plots are given in a linear scaling, in contrast to logarithmically scaled ones on Fig. (**6a**) what makes it worth noticing that the 2nd, and 3rd Raman peaks on figures (**b**) and (**c**) look much more pronounceable comparing the same ones shown on Fig. (**5**) in a logarithmic scale).

The dependence of the SC bandwidth versus the incident pulse energy along with the threshold as a function of the HCF length is plotted in Fig. (**7**). These plots show the SC bandwidth to be a growing function of the pulse energy that exponentially blows up near the SC threshold and obviously becomes saturated as it comes to the longer pieces of the fiber [see Fig. (**7a**)]. Then, it seems only natural the energy threshold decrease at increasing the fiber length [see Fig. (**7b**)].

Notice that a slightly less saturation level of the SC spectral width for the longest HCF [compare, e.g., the curves for L = 95 and L = 245 cm in Fig. (**7a**)] originates from higher attenuation, for lengthy samples, in the fiber silica host, which, in turn, stems from OH absorption near 900 and 1400 nm; see also Fig. (**3a**) and the discussion thereafter where we have revealed a similar fact for the transmission spectra of our HCF as a whole.

Finally, we suggest a demonstration (see Fig. **8**) of what is the spatial distribution of the SC generated in our HCF. That is, we measure the output beam intensity from the rear facet of the HCF which cladding's secondary cores generate the SC. These measurements are done by translating a small-area photo-detector (*Red Wave D123*, which is sensitive to

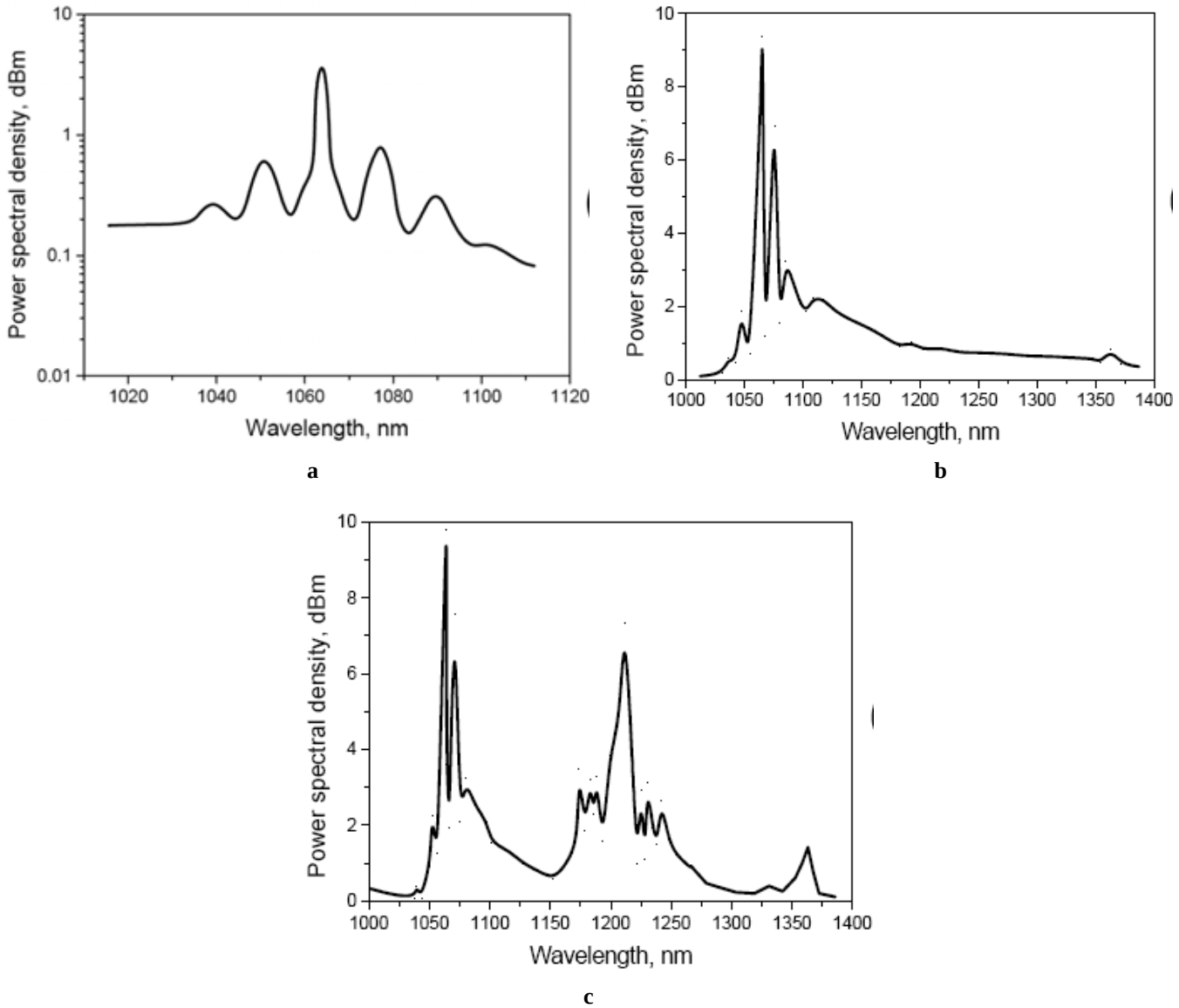

Fig. (6). SC spectra generated in HCF (L = 191 cm) at three different incidence pulse energies: (**a**) 2, (**b**) 5, and (**c**) 10 μJ.

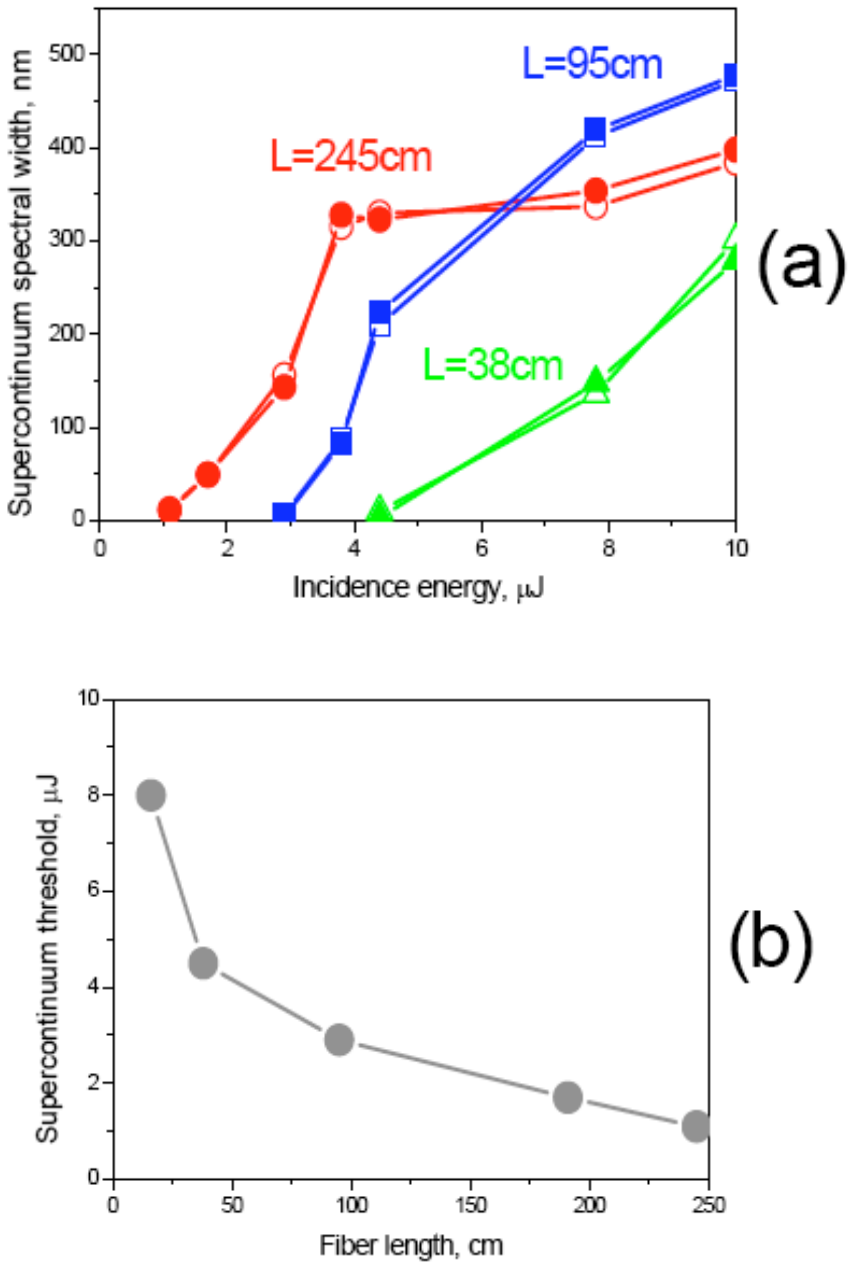

Fig. (7). Dependencies of (**a**) SC spectral width *versus* pump pulse energy, each measured twice (at the SC spectra's half-height, see Fig. **5**) for different HCF lengths) and (**b**) SCG threshold *versus* HCF length.

the radiation at wavelengths from 0.9 to 2.5 μm) perpendicularly to the light beam emerging the fiber sample; a Si filter is placed between the fiber end and the photo-detector to provide a 100%-cutting of the rest of 1.064-μm pump and so to make sure the detected signal 100-% correspondence to the SC (within 1.1–1.4 μm). The detected signals are recorded on an oscilloscope *Instek GQS-620*.

The SC radial distribution recorded at the distance of Z = 2.1 cm from the HCF cleaved end is shown in Fig. (**8a**). It is seen that the SC beam has almost a Gaussian distribution; the SC beam diameter extracted from these data turned out to be about 3.0 μm. For a comparison, Fig. (**8b**) shows the profile of the rest of 1.064-μm pump taken at the same distance from the fiber end in the absence of the Si-filter in front of it; the calculated pump beam diameter in the last case is about 2.5 μm. Needless to say the measured values are very close to the characteristic size of secondary triangle cores of the HCF cladding (~3.0 μm, see above Section 2).

Notice that the fine (micrometric) orthogonal displacement of the HCF sample end with respect to the pump focus position (see Fig. **4**) resulted in a sequential "hops" up and down of the SC signal, that evidently justifies a tight focusing of the pump into one of the triangles (secondary cores) of the HCF cladding, or into the cladding hole pitch – in the case of the SC signal disappearance. Finally, it is worth noticing the SCG in our HCF also happened to be

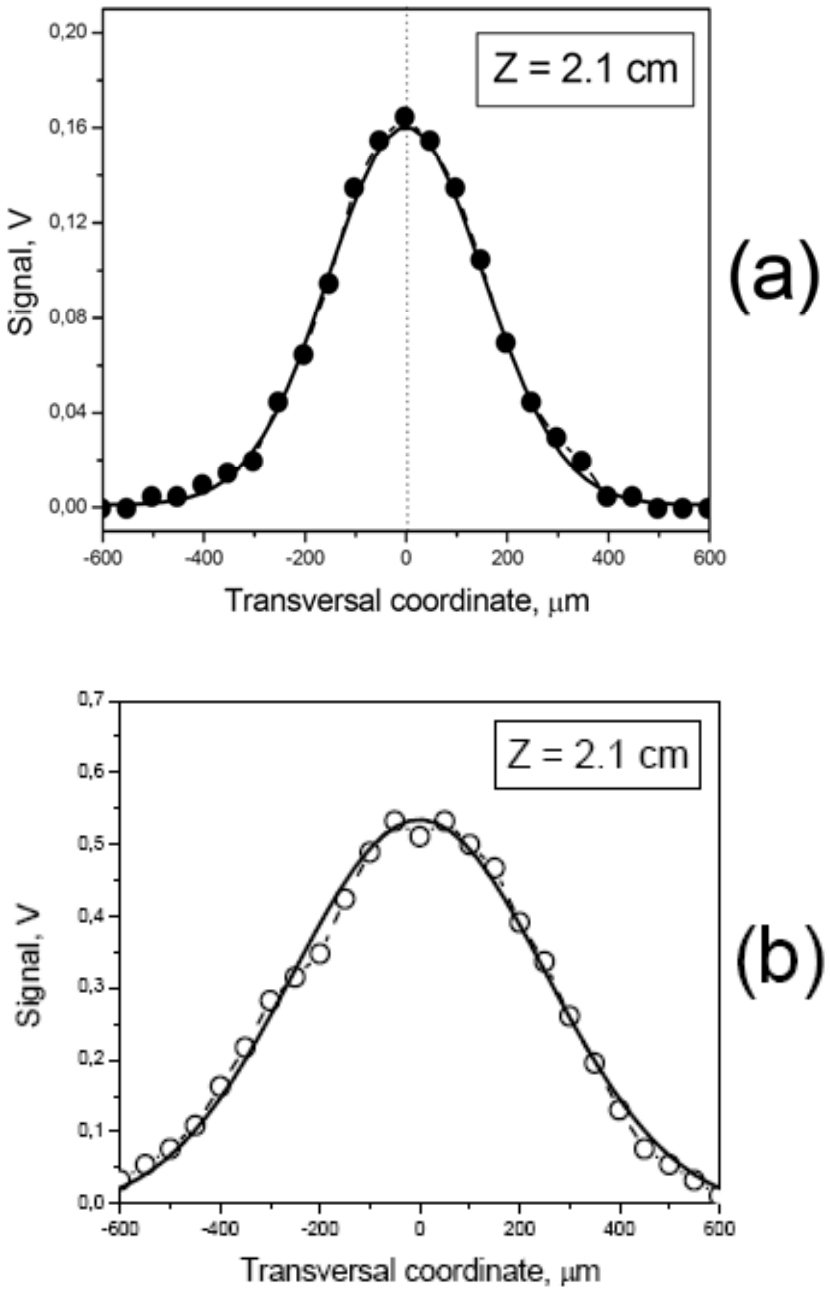

Fig. (8). Transversal distributions of (**a**) SC beam and (**b**) rest of the pump beam at the HCF (L = 245 cm) output. The distance between the fiber rear end and Ge photo-detector is Z = 2.1 cm in both cases.

sensitive to the pump polarization (actually, the SCG generation in the fiber is switched on at a definite orientation of the pump beam polarization when the latter is coincident with one of the fiber birefringence axes provided by its cladding hexagonal structure), and so might be considered as a useful tool to illuminate the role of the fiber birefringence for the SCG to trigger.

4. CONCLUSIONS

One of the key challenges in developing an efficient broadband coherent source is to combine a PCF engineered with well-pronounced non-linear optical properties with a high-peak power laser. Here we present the results of our most recent experiments for the near-IR SCG in a HCF. We demonstrate that a 1-ns microchip laser can produce high-quality, powerful, half-octave near-IR output in such a fiber. To the best of our knowledge, this is the first demonstration of the SCG in the HCF cladding at 1-ns range 1.06-μm excitation. Notice that SCG is attainable at quite short fiber lengths (tens of cm) and is characterized by fairly low threshold of few μJ.

As the HCF fabricated has air-filled 7.5-μm central core and the silica nodes (or "secondary cores") that separate 5-μm holes of the cladding have smaller characteristic size of ~3 μm, their ability of broadband generation are dominated by the nonlinear response of the secondary cores. As our modeling shows, the SCG is more effective in triangular silica nodes of cladding of the developed HCF than in an

equivalent regular single core of a PCF, because of a geometry factor. In turn, the hollow core is demonstrated to provide transmission of light in a linear regime at a wavelength properly managed at the fiber modeling and fabrication.

In conclusion, HCF with few-micron secondary silica cores cladding is fabricated where each of them can serve a source of a smooth half-octave SCG at in-core ~1–10 μJ/ns 1.06 μm excitation with a controllable (1–10 kHz) repetition rate. To the best of our knowledge, this is the first demonstration of SCG in HCF cladding after excitation with a high-peak power microchip laser. The entire configuration is convenient for the implementation of extremely compact monolithically integrated pulsed SC-sources. Tight focusing into a single secondary core is the prerequisite of the SCG (provided by a properly engineered GVD) and, along with the hollow core width, offers the possibility for coupling of different-color lasers into the fiber. It should be noted that other points of interest such as leakage of the SC and delivering lights through the fiber length and guiding efficiency have remained out of the present work scope and will be reported elsewhere.

ACKNOWLEDGEMENTS

The authors would like to thank S. Klimentov, D. Klimentov, A. Levchenko, and L. Sotskaya for valuable contribution into this research.

REFERENCES

[1] Genty G, Coen S, Dudley JM. Fiber supercontinuum sources. J Opt Soc Am B 2007; 24: 1771-85.

[2] Mollenauer LF. Nonlinear optics in fibers. Science 2003; 302: 996-7.

[3] See, E.G. Available from: http://www.crystal-fibre.com/products/nonlinear.shtm

[4] Price JHV, Belardi W, Monro TM, Malinowski A, Piper A, Richardson DJ. Soliton transmission and supercontinuum generation in holey fiber, using a diode pumped Ytterbium fiber source. Opt Express 2002; 10: 382-7.

[5] Lesvigne C, Couderc V, Tonello A, *et al.* Visible supercontinuum generation controlled by intermodal four-wave mixing in microstructured fiber. Opt Lett 2007; 32: 2173-5.

[6] Tombelaine V, Lesvigne C, Leproux P, *et al.* Ultra wide band supercontinuum generation in air-silica holey fibers by SHG-induced modulation instabilities. Opt Express 2005; 13: 7399-404.

[7] Nishizawa N, Takayanagi J. Octave spanning high-quality supercontinuum generation in all-fiber system. J Opt Soc Am B 2007; 24: 1786-92.

[8] Knight JC, Broeng J, Birks TA, Russell PStJ. Photonic band gap guidance in optical fibers. Science 1998; 282: 1476-8.

[9] Cregan RF, Mangan BJ, Knight JC, *et al*. Single-mode photonic band gap guidance of light in air. Science 1999; 285: 1537-9.

[10] Ouzounov DG, Ahmad FR, Muller D, *et al.* Generation of megawatt optical solitons in hollow-core photonic band-gap fibers. Science 2003; 301: 1702-4.

[11] Lin C, Stolen RH. New nanosecond continuum for excited-state spectroscopy. Appl Phys Lett 1976; 28: 216-8.

[12] Russell PStJ. Photonic crystal fibers. Science 2003; 299: 358-62.

[13] Bjarklev A, Broeng J, Bjarklev AS. Photonic Crystal Fibres. Kluver Academic Publishers: Boston; 2003.

[14] Russell PStJ. Photonic-crystal fibers. J Lightw Technol 2006; 24: 4729-49.

[15] Herrmann J, Griebner U, Zhavoronkov N, *et al.* Experimental evidence for supercontinuum generation by fission of higher-order solitons in photonic fibers. Phys Rev Lett 2002; 88: 173901.

[16] Ranka JK, Windeler RS, Stentz AJ. Visible continuum generation in air-silica microstructure optical fibers with anomalous dispersion at 800 nm. Opt Lett 2000; 25: 25-27.

[17] Dudley JM, Provino L, Glossard N, *et al.* Supercontinuum generation in air-silica microstructured fibers with nanosecond and femtosecond pulse pumping. J Opt Soc Am B 2002; 19: 765-71.

[18] Coen S, Chau AHL, Leonhardt R, *et al.* Supercontinuum generation by stimulated Raman scattering and parametric four-wave mixing in photonic crystal fibers. J Opt Soc Am B 2002; 19: 753-64.

[19] Town GE, Funaba T, Ryan T, Lyytikainen K. Optical supercontinuum generation from nanosecond pump pulses in an irregularly microstructured air-silica optical fiber. Appl Phys B 2003; 77: 235-8.

[20] Travers JC, Kennedy RE, Popov SV, Taylor JR, Sabert H, Mangan B. Extended continuous-wave supercontinuum generation in a low water-loss holey fiber. Opt Lett 2005; 30: 1938-40.

[21] Dudley JM, Genty G, Coen S. Supercontinuum generation in photonic crystal fiber. Rev Mod Phys 2006; 78: 1135-84.

[22] Zheltikov AM. Microstructure optical fibers for a new generation of fiber-optic sources and convertors of light pulses. Uspekhi Fizicheskikh Nauk 2007; 171: 737-62.

[23] Knight JC. Photonic crystal fibers and fiber lasers. J Opt Soc Am B 2007; 24: 1661-9.

[24] Russell P. Photonic crystal fiber: finding the holey grail. Opt Photon News 2007; 18 (7): 26-31.

[25] Dupriez P, Poletti F, Horak P, *et al*. Efficient white light generation in secondary cores of holey fibers. Opt Express 2007; 15: 3729-36.

[26] Minkovich VP, Kir'yanov AV, Sotsky AV, Sotskaya LI. Large-mode-area holey fibers with a few air channels in cladding: modeling and experimental investigation of the modal properties. J Opt Soc Am B 2004; 21: 1161-9.

[27] Bredol M, Leers D, Bosselaar L, Hutjens M. Improved model for OH absorption in optical fibers. J Light Technol 1990; 8: 1536-9.

[28] Klimentov SM, Kir'yanov AV, Mel'nikov IV, Powers PE. Compact source based on a microchip laser and periodically poled lithium niobate. Technical Digest: International Conference "CLEO/Europe IQEC 2007". Munich, Germany, 2007; pp. CA9-3-THU.

Received: February 05, 2010 Revised: March 03, 2010 Accepted: May 12, 2010